Cytokeratins 8 and 19 in the Mouse Placental Development

Yoshitaka Tamai,* Tomo-o Ishikawa,* Michael R. Bösl,* Masahiko Mori,‡ Masami Nozaki,§ Heléne Baribault,‖ Robert G. Oshima,‖ and Makoto M. Taketo¶

*Banyu Tsukuba Research Institute (Merck), Tsukuba, Ibaraki 300-2611, Japan; ‡National Institute of Radiological Sciences, Inage-ku, Chiba 263-8555, Japan; §Research Institute for Microbial Diseases, Osaka University, Suita, Osaka 565-0871, Japan; ‖The Burnham Institute, La Jolla, California 92037; and ¶Graduate School of Pharmaceutical Sciences, University of Tokyo, Bunkyo-ku, Tokyo 113-0033, Japan

Abstract. To investigate the expression and biological roles of cytokeratin 19 (K19) in development and in adult tissues, we inactivated the mouse K19 gene (*Krt1-19*) by inserting a bacterial β-galactosidase gene (*lacZ*) by homologous recombination in embryonic stem cells, and established germ line mutant mice. Both heterozygous and homozygous mutant mice were viable, fertile, and appeared normal. By 7.5–8.0 days post coitum (dpc), heterozygous mutant embryos expressed *lacZ* in the notochordal plate and hindgut diverticulum, reflecting the fact that the notochord and the gut endoderm are derived from the axial mesoderm-originated cells. In the adult mutant, *lacZ* was expressed mainly in epithelial tissues. To investigate the possible functional cooperation and synergy between K19 and K8, we then constructed compound homozygous mutants, whose embryos died ∼10 dpc. The lethality resulted from defects in the placenta where both K19 and K8 are normally expressed. As early as 9.5 dpc, the compound mutant placenta had an excessive number of giant trophoblasts, but lacked proper labyrinthine trophoblast or spongiotrophoblast development, which apparently caused flooding of the maternal blood into the embryonic placenta. These results indicate that K19 and K8 cooperate in ensuring the normal development of placental tissues.

Key words: embryo • endoderm • epithelium • keratin • trophoblasts

Introduction

Cytokeratin-intermediate filaments are encoded by a multigene family of ∼20 related polypeptides. They are expressed mainly in epithelial cells depending on the extent of differentiation (Moll et al., 1982). Cytokeratin proteins are classified into two types: smaller and acidic type I, and larger and more basic type II (Steinert and Roop, 1988). In simple epithelia, they form cytokeratin filaments through obligate heteropolymerization of the type I and type II proteins in particular combinations. For example, cytokeratin 8 (K8)[1] and cytokeratin 18 (K18); K8, K18, and K19; or cytokeratin 7 (K7), K8, K18 and K19 (Moll et al., 1982; Lane et al., 1983; Sun et al., 1984; Quinlan et al., 1985). The smallest type I cytokeratin, K19 (Mr; 40 kD) was first recognized as a distinct form in squamous cell carcinoma lines (Wu and Rheinwald, 1981). Cytokeratins share a common structural organization: a central α-helical rod domain flanked by head and tail domains. Although K19 has a highly conserved central α-helical rod essential for filament formation (Steinert and Roop, 1988) and the head domain, it is distinguished from other cytokeratins by lacking a tail domain (Bader et al., 1986; Ichinose et al., 1989; Lussier et al., 1989; Stasiak et al., 1989). The gene encoding mouse K19 (*Krt1-19*) is located on chromosome 11, in the immediate neighborhood of the K15 gene (*Krt1-15*), separated by only 4 kb (Lussier et al., 1990; Nozaki et al., 1994). The human K19 gene (*KRT19*) is located on chromosome 17 (Bader et al., 1988). While K19 and K15 are coexpressed in certain cell types, they are not in others (Ichinose et al., 1989; Nozaki et al., 1994). K19 is one of the most representative proteins of epithelial cells such as those in the intestine, kidney collecting ducts, gallbladder, mesothelium, and secretory glands (Moll et al., 1982; Sun et al., 1984; Quinlan et al., 1985; Bosch et al., 1988). In the mouse blastocyst trophectoderm, K19 is induced after K8 and K18 upon implantation (Jackson et al., 1980; Nozaki et al., 1988; Takemoto et al., 1991; Tamai et al., 1991). In the mouse embryo proper, K19 mRNA becomes detect-

Address correspondence to Makoto Mark Taketo, Laboratory of Biomedical Genetics, Graduate School of Pharmaceutical Sciences, University of Tokyo, Bunkyo-ku, Tokyo 113-0033, Japan. Tel.: 81-3-5841-4859. Fax: 81-3-5841-4778. E-mail: taketo@mol.f.u-tokyo.ac.jp.

Dr. Ishikawa's present address is Department of Pharmacology, Graduate School of Medicine, Kyoto University, Sakyo-ku, Kyoto 606-8501, Japan. Dr. Bösl's present address is Zentrum für Molekulare Neurobiologie, Universität Hamburg, Hamburg, D-20246, FRG. Dr. Baribault's present address is Deltagen Inc., San Carlos, CA 94061.

[1]*Abbreviations used in this paper:* dpc, days post coitum; ES, embryonic stem; K, cytokeratin.

able by 9.5 days post coitum (dpc) (Lussier et al., 1989), and is probably expressed earlier (Jackson et al., 1981; Franke et al., 1982). Differentially expressed individual cytokeratins, including K19, are remarkably stable markers in various types of carcinomas even when other markers have been lost (Kasper et al., 1987; Pujol et al., 1993; Moll, 1994). Accordingly, cytokeratins are used for carcinoma subtyping regarding the extent of differentiation and their origins, especially for metastatic foci. Progress has been made in understanding the functions of cytokeratins in the skin. Point mutations in cytokeratin genes (Fuchs, 1994; McLean and Lane, 1995) and transgenic (Vassar et al., 1991) or knockout mice have indicated a structural function for epidermal keratins (for a review, see Magin, 1997). Homozygous mutant embryos for the simple epithelia type K8 gene (*Krt2-8*) are retarded in growth and suffer from internal bleeding, with an abnormal accumulation of erythrocytes in the fetal liver (Baribault et al., 1993, 1994). These alterations are consistent with a placental or extraembryonic deficiency. While this mutation shows a 94% penetrance in the C57BL/6 background, the proportion of viable homozygotes increases in the FVB/N background, and colorectal hyperplasia and inflammation are observed in adults that escape embryonic lethality. Recently, K8 and K18 have been shown to confer resistance to tumor necrosis factor–induced apoptosis (Caulin et al., 2000). Based on its structure and tissue distribution, K19 has been suggested to counterbalance type II keratins (Ecker, 1988; Stasiak et al., 1989). To determine the expression pattern and function of K19, we have constructed a *Krt1-19* null mutant allele by knocking in a *lacZ* cassette at the translation initiation site. We also generated compound homozygotes of *Krt1-19* and *Krt2-8* mutations and found that homozygous embryos are not viable due to defective placental tissues, a phenotype not observed in the simple homozygous mutants.

Materials and Methods

Construction of a Krt1-19 Targeting Vector

A λ recombinant clone containing the mouse *Krt1-19* was isolated from a 129/Sv genomic library using a 1.4-kb full-length K19 cDNA fragment as a probe as previously characterized (Ichinose et al., 1989; Nozaki et al., 1994). A 6.5-kb SalI–KpnI fragment containing a part of exon 1 and a 641-bp KpnI–BglII fragment downstream from a KpnI site in exon 1 were excised from this recombinant phage and subcloned in the pUC19 vector. The ATG translation initiation codon in exon 1 was converted to a KpnI site. A 365-bp KpnI fragment in exon 1 was replaced with a cassette containing a *lacZ* reporter and PGKneobpA (Soriano et al., 1991). Thus, the targeting vector pJBX carried a long homology arm of 6.1 kb.

Transfection of Embryonic Stem Cells and Selection of Targeted Clones

D3a2 embryonic stem (ES) cells (Shull et al., 1992) were cultured on neomycin-resistant (neo^r) mouse embryonic fibroblasts (Oshima et al., 1995). 50 μg of the targeting vector were linearized at the unique Sse8387I site and electroporated into 10^7 ES cells at 250 V and 500 μF. 24 h later, 150 μg/ml (titer) of G418 (Geneticin; Sigma-Aldrich) was added. 7 d later, single colonies were isolated and cultured in duplicate. G418-resistant colonies were screened for homologous recombination by PCR using oligonucleotide primers: one complementary to neo^r; PGK^r (5′-CTA AAG CGC ATG CTC CAG ACT-3′) and the other located 92-bp downstream from the 3′ BglII site in *Krt1-19*; K19-R2G (5′-AAG AGC TCC CTG ACT AGA TTC AAG TTA ACT-3′). 35 cycles of amplification were performed (denaturation, 1 min at 94°C; hybridization, 2 min at 60°C; and elongation, 2 min at 72°C) in 50 μl reaction mixtures containing 50 pmol of each oligonucleotide, 1 U Taq polymerase (TAKARA), 0.5 U Perfect Match® (Stratagene), and 1 μl of the crude cell lysate in each mixture. As shown in Fig. 1 (below), only homologous recombinants showed a 739-bp band. Candidates for homologous recombinants were expanded and verified by Southern hybridization with probes either internal (a 630-bp PstI–XbaI fragment containing the neo^r segment of pPGKneobpA) or external (a 556-bp fragment located downstream from the 3′ BglII site) to the targeting vector sequence.

Generation and Genotyping of the Mutant Mice

Chimeras were generated by injection of the ES cells into C57BL/6 (B6) blastocysts, followed by transfers to MCH (CLEA) foster mothers. Chimeric mice were backcrossed to B6 mice, and germ line transmission was determined by the presence of the agouti coat color. Heterozygous offsprings were identified by PCR and Southern analysis of tail DNA samples. Tail tips were incubated in lysis buffer of SepaGene® (Sankojunyaku), in the presence of 1 mg/ml proteinase K overnight at 55°C. DNA was extracted according to the manufacturer's protocol. The wild-type allele was identified using two primers sandwiching the deleted portion of exon 1 (sense primer, endo-F: 5′-CCT GAC TAG ATT CAA GTT AAC TG-3′, and antisense primer, endo-R: 5′-TGG CGG AGT CCG CGG TGG AAG TT-3′). 35 cycles (denaturation, 1 min at 94°C; annealing, 2 min at 60°C; and elongation, 2 min at 72°C) were performed to amplify the 958-bp fragment. The *Krt2-8* alleles were identified as described before (Baribault et al., 1994).

Histochemical Localization of the β-Galactosidase Activity

For the timing of embryos, the morning of the vaginal plug was considered as 0.5 dpc. When removed from the decidua, embryos were staged according to Kaufman (1992) and genotyped as described above using DNA extracted from the yolk sac or from the embryo itself. To detect the β-galactosidase activity, the samples were incubated at 30°C for 30 min to 3 h, depending on their sizes in a staining solution (5 mM potassium ferricyanide, 5 mM potassium ferrocyanide, 1 mg/ml X-gal in PBS). For paraffin sectioning, samples were fixed in 4% paraformaldehyde according to the standard procedures.

Immunohistochemistry

For immunofluorescence staining, tissues were fixed in 100% methanol at 4°C for 10 min, rinsed in PBS, and embedded in the O.C.T. compound. The frozen sections were prepared at 20-μm thickness, followed by incubation in 0.3% H_2O_2/PBS for 30 min at room temperature. Sections of embryos and adult tissues were incubated with a blocking solution (3% BSA, 5% goat serum, and 0.2% Triton X-100 in PBS) for 1 h at room temperature. The primary antibodies TROMA-1, -2, and -3 raised against K8, K18, and K19, respectively, were obtained from Dr. Kemler (Max-Planck Institute of Immunology, Freiburg, Germany; Kemler et al., 1981; Boller et al., 1987), and were used at a dilution of 1:10 and incubated with the specimens for 1 h at room temperature. Antibodies against K7 and Kip2 were purchased from Euro-Diagnostica and Santa Cruz Biotechnology, Inc., respectively. Sections were washed, and then incubated with FITC-conjugated secondary antibodies (Amersham, UK). For peroxidase-coupled reactions, tissues were fixed in 4% paraformaldehyde or 70% ethanol and embedded in paraffin. Sections were incubated with peroxidase-conjugated secondary antibodies (Amersham Pharmacia Biotech) using a substrate kit (Vector Laboratories) according to the manufacturer's protocol.

In Situ Hybridization of Whole Mount Embryos

Whole mount in situ hybridizations of the 9.0–9.5-dpc embryos were carried out as described previously (Saga et al., 1996) using digoxigenin-UTP–labeled single-strand RNA probe. The K19 probe was transcribed from a K19 cDNA fragment (Ichinose et al., 1989).

Results

Disruption of the Mouse K19 Gene (Krt1-19) by Homologous Recombination in ES Cells

To construct *Krt1-19* knock out mice, one of the *Krt1-19* alleles was inactivated by homologous recombination in ES

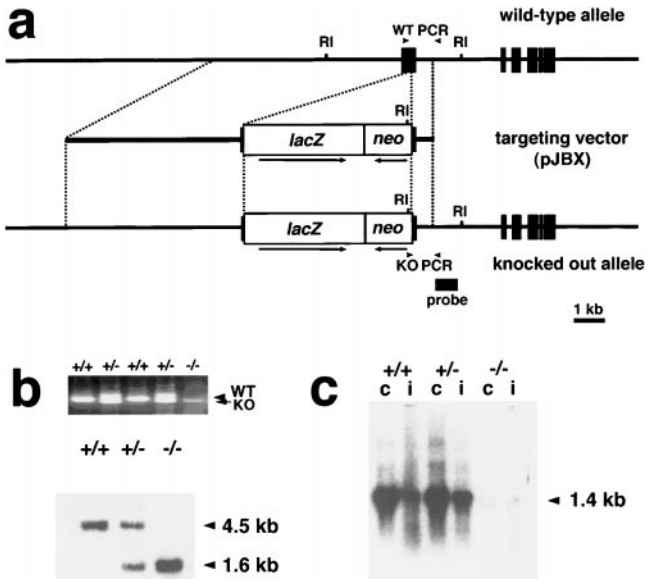

Figure 1. Inactivation of the mouse K19 gene (*Krt1-19*) by homologous recombination. (a) Structures of the wild-type allele, targeting vector pJBX, and the targeted allele. The targeting vector contained two regions of homology to the genomic DNA, sandwiching a *lacZ* reporter-neo selection cassette. Homologous recombination resulted in deletion of most of exon 1, and the *lacZ* reporter was transcribed from the *Krt1-19* promoter. Filled boxes represent exons; noncoding regions are shown as solid lines. Arrowheads indicate the positions of the PCR primers for genotyping: KO PCR, primers for the targeted allele, and WT PCR, primers for the wild-type allele. The probe for Southern hybridization is shown as a solid line. RI, EcoRI site. Arrows beneath the *lacZ* reporter-neo selection cassette show the transcriptional directions. (b) Genotype analysis of the wild-type, heterozygous, and homozygous mutant mouse tail DNAs. (Top) Transmission of the targeted allele to the progeny as determined by PCR. KO, targeted allele (739 bp); WT, wild-type allele (958 bp). (Bottom) Southern hybridization analysis. The EcoRI fragments of 4.5 and 1.6 kb derived from the wild-type and targeted alleles, respectively. (c) Northern hybridization analysis of K19 mRNA in the wild-type, heterozygous, and homozygous mice. 10 μg of the total RNA purified from the colon (c), or small intestine (i) were loaded in each lane and probed with a K19 cDNA probe (Ichinose et al., 1989). The arrowhead indicates the size of the K19 mRNA (1.4 kb).

Table I. Genotype Analysis of Krt1-19 Heterozygous Intercrosses

	Offspring genotype			
Parent strains	+/+	+/−	−/−	Total
F_1*	24	62	29	115
C57BL/6 (N_1)‡	18	36	10	64
C57BL/6 (N_2)‡	7	17	11	35
FBV/N (N_1)‡	25	28	6	59
FBV/N (N_2)‡	14	35	8	57

Numbers indicate pups from each set of intercrosses.
*Heterozygous crosses between parents in the C57BL/6 and 129/Sv backgrounds.
‡N_1 and N_2 indicate the backcross numbers of the parents.

cells. The translation initiation site of *Krt1-19* was disrupted so that a bacterial *lacZ* gene was placed under the control of the *Krt1-19* promoter (Fig. 1 a). 200 G418-resistant clones were analyzed, and three independent homologous recombinant candidates were isolated. Homologous recombination in these ES clones were verified further by PCR and Southern analyses (Fig. 1 b). All three recombinant ES lines were injected into C57BL/6 (B6) blastocysts and two germ line chimeras were generated. About half of their agouti offspring carried the knockout allele. The heterozygous mutant mice were viable, fertile, and appeared normal.

Upon intercrosses of heterozygous mutants, the distribution of the wild type (+/+), heterozygous (+/−), and homozygous (−/−) mice were not significantly different from the expected Mendelian ratio in the F_1 and B6 backcross mice (Table I). In the FBV/N backcross offspring, however, the homozygote numbers were smaller than expected ($P < 0.05$). While the reason for this phenomenon remains to be investigated, the FVB/N K19 mutant was maintained thereafter as homozygotes because they survived and reproduced without affecting the litter size or the sex ratio (data not shown). The homozygous *Krt1-19* mutants did not show any particular phenotypic changes, and appeared identical to their heterozygous and wild-type littermates in their gross anatomy, histology, and behavior. Up to the age of 20 mo, we have not observed any difference in changes associated with aging.

To investigate K19 expression in the mutant mice, RNA samples from the small intestine and colon of the homozygous, heterozygous, and wild-type mice were analyzed by Northern hybridization (Fig. 1 c). The knockout mutation

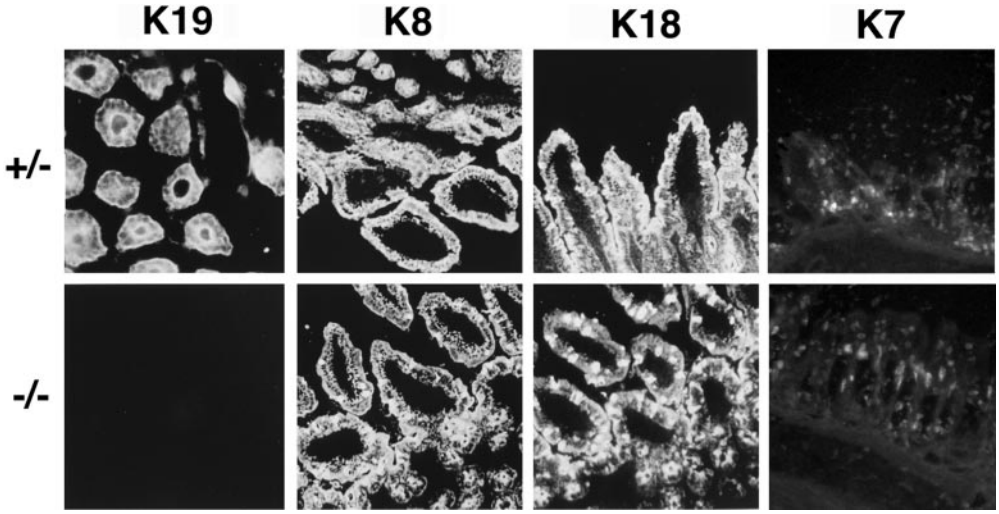

Figure 2. Immunofluorescence staining of K19, K8, K18, and K7 in the K19 gene heterozygous and homozygous mutant mouse intestines. Frozen sections of the adult mice were fixed with methanol and stained with TROMA-3 (anti–K19), -1 (anti–K8), and -2 (anti–K18), and an anti–K7 mAb.

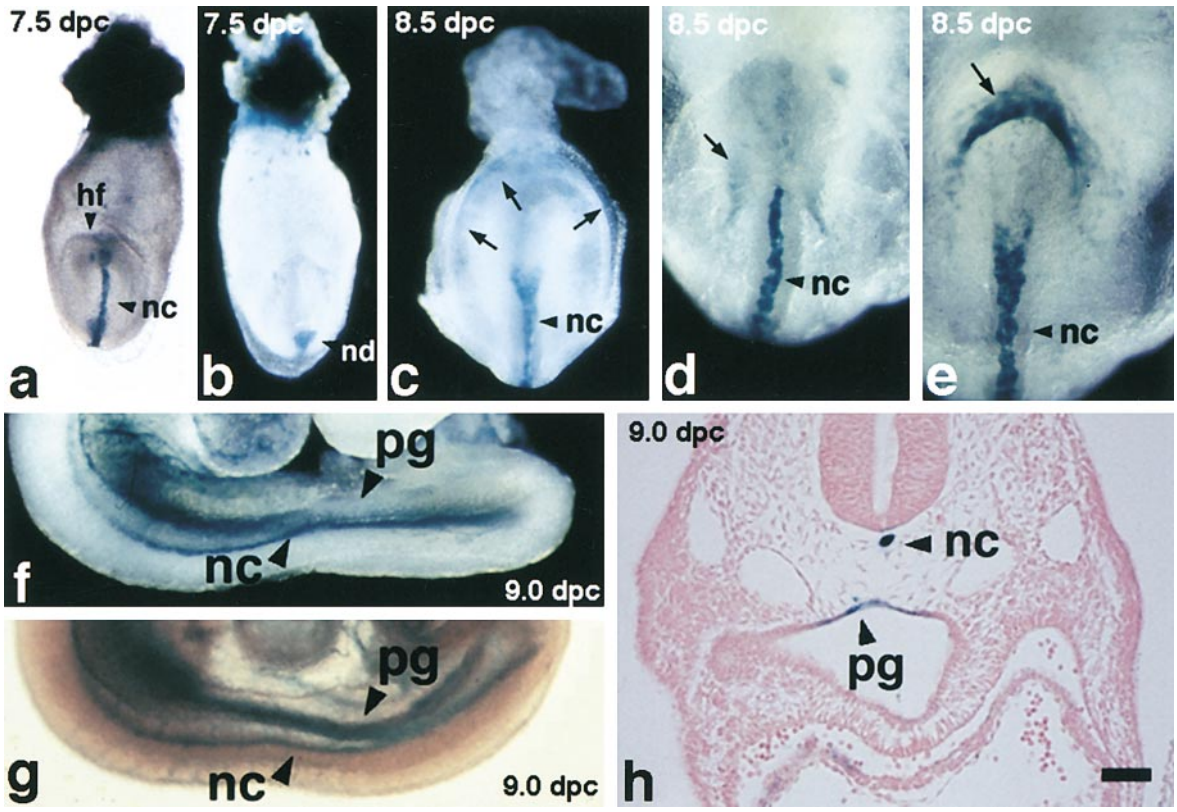

Figure 3. Expression of the β-galactosidase gene (*Krt1-19-lacZ*) in the heterozygous mouse embryos at 7.5–9.0 dpc. (a and b) A representative embryo at 7.5 dpc in the anterior and posterior views, respectively. Note the β-galactosidase activity in the notochordal plate, node, and ectoplacental cone. (c) A representative embryo at 8.5 dpc in the posterior view. Note the β-galactosidase activity in an arch pattern (arrows). (d and e) Another embryo at 8.5 dpc in the anterior (d) and posterior (e) views. Note that this embryo is more progressed in development than that in c: the arch pattern of the β-galactosidase staining at the hindgut (e, arrows) is much smaller than that seen in the embryo shown in c. Also note the staining inside the foregut in d (arrow). (f and g) A representative embryo at 9.0 dpc. (h) A transverse section of the same embryo shown in f and g (Eosin counterstaining). hf, head fold; nc, notochordal plate; nd, node; pg, primitive gut. All dissection micrographs (whole mount in situ staining) were taken under a dark-field illumination, except a and g, which were in a bright field. Bar, 100 μm.

abolished the K19 mRNA in the small intestine and colon. The levels of the mRNAs for K8 that complexes with K19, and for K18, another type-I cytokeratin, were essentially unaffected in both heterozygous and homozygous mutants (data not shown). As expected, no K19 protein was detected in the homozygous tissues by Western immunoblot analysis with specific antibody TROMA-3 (data not shown). As shown in Fig. 2, immunofluorescence stainings of the intestinal sections demonstrated no K19 filaments in the homozygous tissues, whereas expression of K8, K18, and K7 proteins remained unaffected. It is worth noting that the K7 staining was observed in goblet cells in both genotypes.

Expression of K19 in Heterozygous Mutants Determined by β-Galactosidase Expression

To monitor K19 expression in various tissues, the targeting vector was designed so that a *lacZ* reporter gene was driven by the *Krt1-19* promoter of the knocked-out allele. We determined the β-galactosidase reporter activity by whole mount in situ staining of various organs and embryos. As expected, simple epithelia of the small intestine, cecum, and colon were stained. In the intestines, not only the villus epithelium, but also the crypts were stained. The squamous epithelium of the esophagus, the hair follicle cells, and some gland cells in the skin also expressed β-galactosidase (data not shown). These results are consistent with the in situ mRNA analysis and immunostaining data published previously (Bosch et al., 1988).

In the preimplantation embryo, the trophectoderm cells of the blastocyst were stained only very weakly with X-gal. In the 6.0-dpc embryos, β-galactosidase was expressed only in the ectoplacental cone. In the 7.0-dpc embryo, the enzyme activity was detected mainly at the ectoplacental cone (data not shown). In the late primitive streak stage, β-galactosidase was expressed in the embryo proper, at the notochordal plate, and the node (Fig. 3, a and b). Shortly after (7.5–8.5 dpc), an arch-shaped staining appeared in the posterior embryo (Fig. 3 c). The diameter of this arch became smaller thereafter and the staining was localized in the hindgut pocket. When the foregut and hindgut invaginations were formed, the endodermal cells lining them expressed β-galactosidase (Fig. 3, d and e). Later (9.0–9.5 dpc), β-galactosidase expression was limited to the primitive gut and the notochord (Fig. 3, f–h). In vivo, cytokeratins are not stable unless type I and type II polypeptides are copolymerized (Kulesh et al., 1989). To confirm the expression patterns monitored by the β-galactosidase activity, the K19 mRNA and protein were analyzed in the embryos. Expression of the endogenous *Krt1-19* gene essentially corresponded to the β-galactosidase

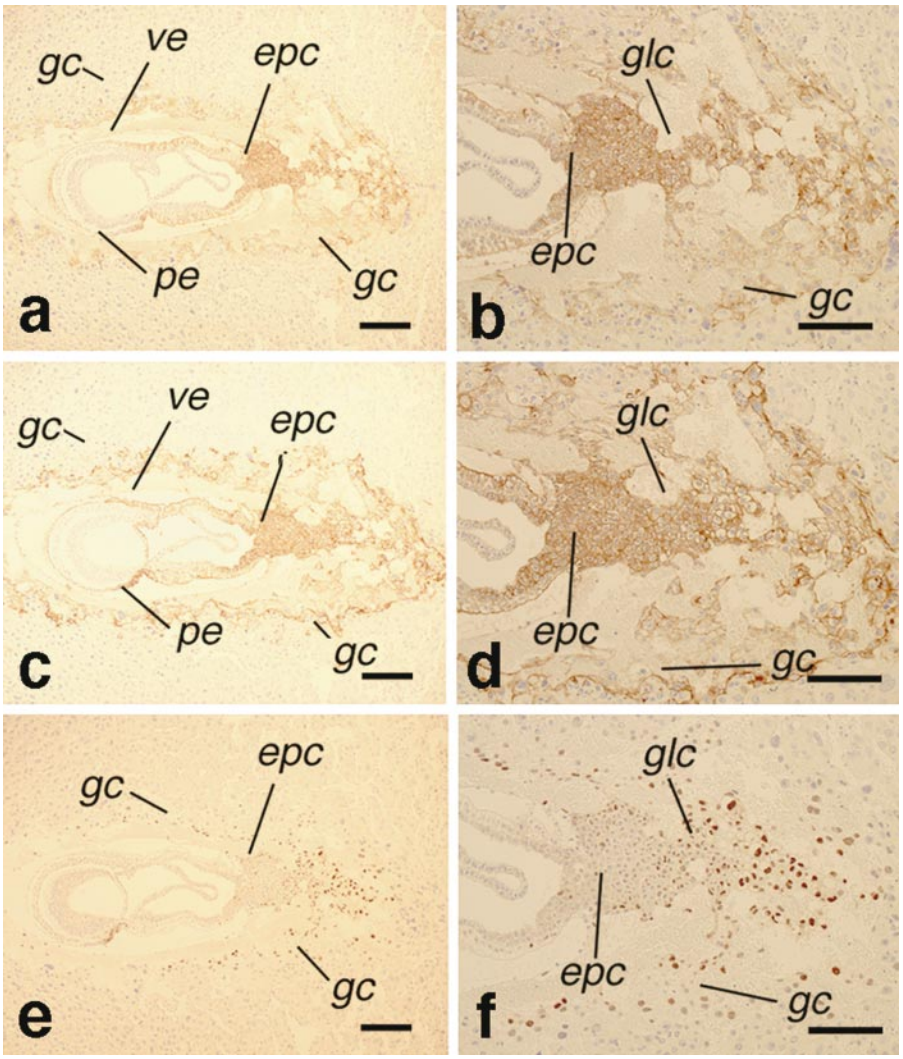

Figure 4. Colocalization of K8 and K19 in the mouse extra embryonic tissues. Immunohistochemical staining of the wild-type embryos in utero at 7.5 dpc with TROMA-3 (anti–K19), TROMA-1 (anti–K8), and anti–Kip2 antibodies. Note that K19 and K8 are expressed in the cytoplasm, whereas Kip2 is in the nucleus. (a and b) Staining for K19. (c and d) Staining for K8. (e and f) Staining for Kip2. epc, ectoplacental cone; gc, giant cells; glc, glycogen cells; pe, parietal yolk sac endoderm; ve, visceral yolk sac endoderm. Note that a, c, and e are serial sections, while b, d, and f are a higher magnification of the sections in a, c, and e, respectively, Bars: a, c, and e, 100 μm; b, d, and f, 50 μm.

activity, although there were subtle differences in the signal intensities (data not shown).

Compound Homozygotes for K8 (Krt2-8) and K19 (Krt1-19) Mutations

To determine the expression patterns of K8 and K19, B6 embryos (6.5–7.5 dpc) were analyzed by immunohistochemistry with TROMA-1 (anti–K8) and TROMA-3 (anti–K19), respectively. As a result, both K8 and K19 proteins turned out to be expressed mostly in the extraembryonic tissues, in almost identical patterns. At 6.5 dpc, both K8 and K19 were expressed mainly in the ectoplacental cone and trophoblasts, although the level of K19 was lower than that of K8 (data not shown). These staining patterns were more obvious and stronger at 7.5 dpc. In addition to ectoplacental cone and giant trophoblasts, glycogen cells, parietal and visceral endoderm cells expressed both K8 and K19 at similar levels (Fig. 4, a–d). On the other hand, Kip2, a marker for the ectoplacental cone and trophoblastic giant cells (Riley et al., 1998), was expressed in the nuclei of these cells, as expected (Fig. 4, e and f). Accordingly, compound homozygous mutants were constructed in the FVB/N background to determine whether K8 and K19 have compensatory functions in vivo. The FVB/N background was chosen because more than half of the K8 gene (*Krt2-8*) homozygotes survive to adults in the FVB/N background (Baribault et al., 1994), although the homozygous null mutation in the B6 background causes an embryonic lethality around 12 dpc (Baribault et al., 1993). First, the F_1 mice from the respective homozygous parents were obtained. These compound heterozygotes [*Krt2-8* (+/−):*Krt1-19* (+/−)] were viable and fertile. When they were intercrossed, however, no compound homozygous pups [*Krt2-8* (−/−):*Krt1-19* (−/−)] were found, although [*Krt2-8* (+/−):*Krt1-19* (−/−)] and [*Krt2-8* (−/−):*Krt1-19* (+/−)] were viable and fertile (data not shown). To determine the stage when the compound homozygous embryos became lethal, the concepti were examined chronologically from the intercrosses of mice that were heterozygous for the K8

Table II. Genotype Analysis of Compound Knockout Crosses

F_1 genotypes	*Krt2-8* (+/+): *Krt1-19* (−/−)	*Krt2-8* (+/−): *Krt1-19* (−/−)	*Krt2-8* (−/−): *Krt1-19* (−/−)	Necrotic or resorption
7.5–9.5 dpc	24	34	18	1
10.5 dpc	14	27	4*	7
11.5–13.0 dpc	5	13	0	9
Postnatal	79	140	0	—

Parents: K8 (*Krt2-8,* +/−):K19 (*Krt1-19,* −/−) × K8 (*Krt2-8,* +/−):K19 (*Krt1-19,* −/−). Parents were after the sixth backcross generation into the FVB/N background.
*Embryos with abnormal morphology.

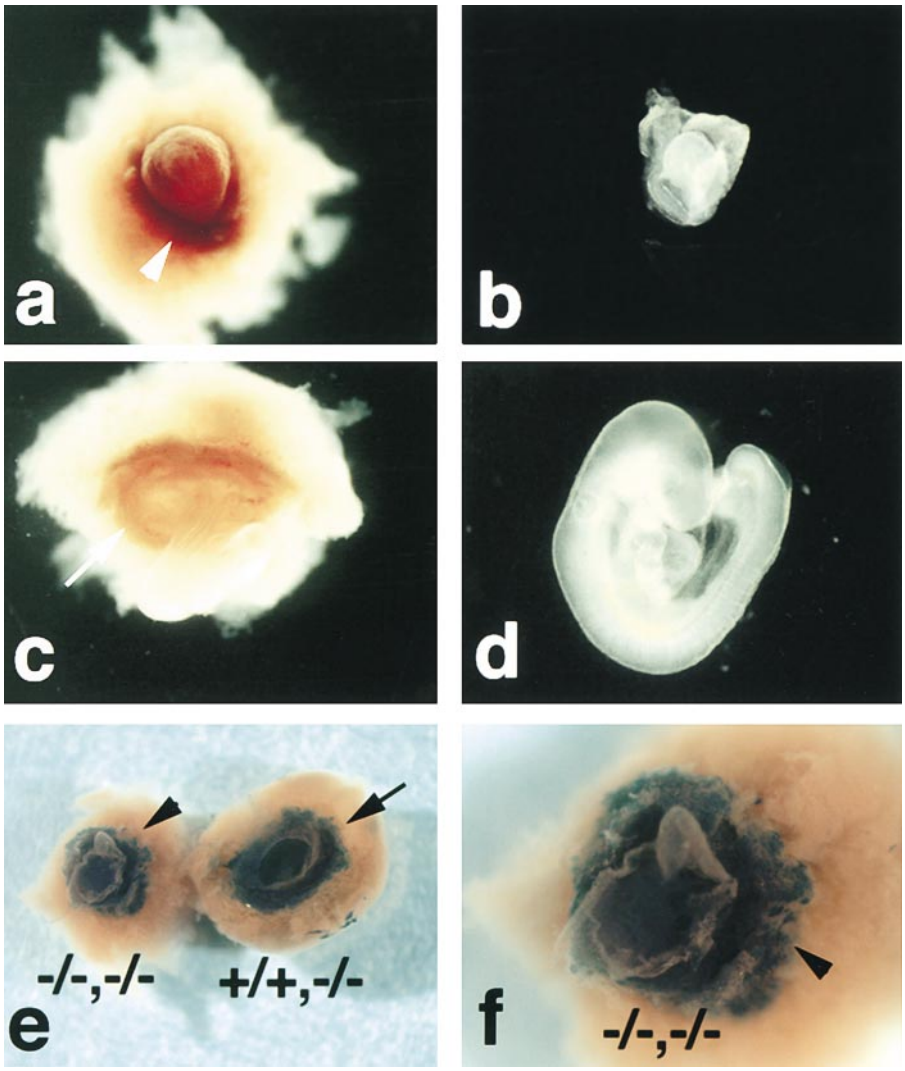

Figure 5. Smaller placentas and embryo growth retardation in the K8/K19 compound homozygous mutant concepti. (a) A *Krt2-8* (−/−):*Krt1-19* (−/−) conceptus at 9.75 dpc. Note a red lesion (arrowhead). (b) A *Krt2-8* (−/−):*Krt1-19* (−/−) embryo, showing a retarded growth. (c) A *Krt2-8* (+/+):*Krt1-19* (−/−) conceptus at 9.75 dpc. Arrow indicates the implantation site. (d) A *Krt2-8* (+/+):*Krt1-19* (−/−) embryo as a control. Note that a and c, and b and d, were photographed at the same magnifications. (e) Comparison of the placenta between a K8/K19 compound homozygote and a simple K19 homozygote, stained for β-galactosidase at 9.75 dpc. (−/−,−/−) Compound homozygote [i.e., *Krt2-8* (−/−):*Krt1-19* (−/−)]; (+/+,−/−) simple K19 homozygote [*Krt2-8* (+/+):*Krt1-19* (−/−)]. (f) A higher magnification of the compound homozygous conceptus in e.

mutation, but homozygous for K19 [*Krt2-8* (+/−):*Krt1-19* (−/−)] (Table II). DNA extracted from fetal membranes or portions of embryos were used for genotyping. As a result, the embryos from 7.5–9.25 dpc showed the Mendelian distribution, and no difference was observed among the [*Krt2-8* (+/+):*Krt1-19* (−/−)], [*Krt2-8* (+/−):*Krt1-19* (−/−)], and [*Krt2-8* (−/−):*Krt1-19* (−/−)] embryos. After 9.5 dpc, however, the number of the compound homozygous embryos decreased gradually, with increasing numbers of necrotic remnants and resorption sites. At 9.75–10.5 dpc, some of the compound homozygous embryos were still alive, but they were easily distinguishable by the smaller size of their embryo-derived portion of the placenta and varying degrees of growth retardation compared with their littermates (Fig. 5).

The most prominent characteristic under a dissection microscope was much more blood at the implantation sites. Histological examination of serial sections of the trophoblastic tissues at 10.5 dpc revealed lesions filled with unnucleated maternal erythrocytes in the placenta of the compound homozygous embryos (Fig. 6, a, c, and e compared with b, d, and f, respectively). Upon closer examination at higher magnifications, the lesions also contained some large and nucleated embryonic erythrocytes as well (e.g., Fig. 6 g, arrows). Compared with the [*Krt2-8* (+/−):*Krt1-19*(−/−)] or [*Krt2-8* (+/+):*Krt1-19* (−/−)] concepti, the placentas of the compound homozygotes contained multiple layers of giant cells without the normal architecture of the labyrinthine trophoblasts or spongiotrophoblasts. The allantois was also formed very poorly (Fig. 6, compare g with h).

To verify the histological findings at 10.5 dpc, and to investigate earlier changes in the compound homozygous placenta, we then investigated the tissues at 9.5 dpc. A trophoblast differentiation marker Kip2 was expressed in the ectoplacental cone, trophoblast giant cells, and diploid trophoblastic cells in the wild-type embryos (Fig. 4, e and f). An immunohistochemical analysis in the compound homozygous placenta showed a marked increase in the number of the secondary giant cells already at 9.5 dpc (Fig. 7, a, c, and e compared with b, d and f, respectively). Moreover, these giant trophoblasts were with much larger cell bodies and nuclei, and they were pulled apart but not tightly attached to each other as in the simple K19 homozygotes. In contrast, the number of the labyrinthine trophoblast and spongiotrophoblast cells were decreased in cell number, and they were poorly organized. This apparently caused flooding of maternal blood directly into the embryonic tissues where these trophoblasts normally separate embryonic blood from the maternal circulation. Therefore, this

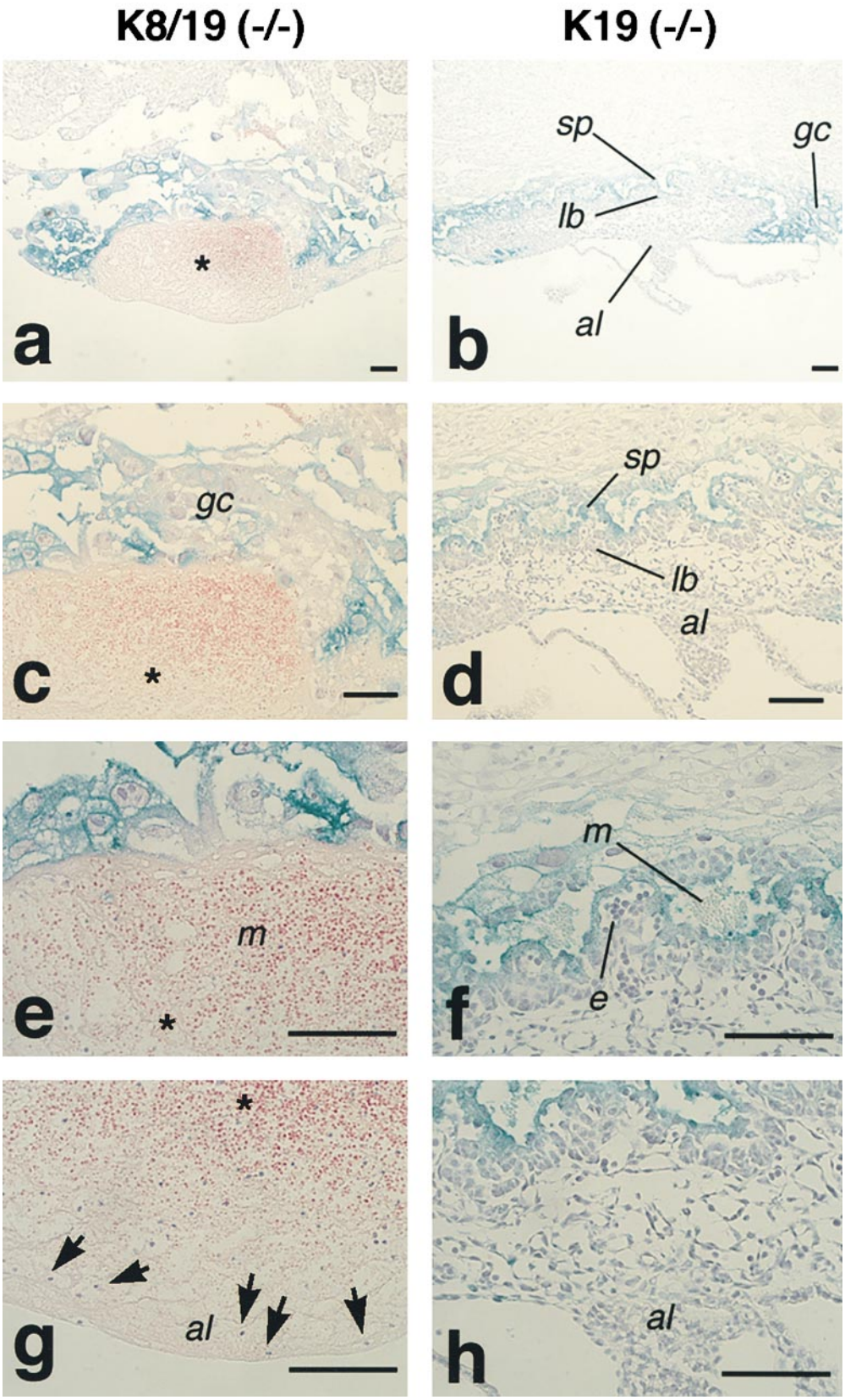

Figure 6. Comparison of the placental regions at 10.5 dpc between the K8/K19 compound homozygotes and simple K19 homozygotes. (Left) Sections from the K8/K19 compound homozygous concepti [*Krt2-8* (−/−):*Krt1-19* (−/−)]. (Right) Sections from the simple K19 homozygous concepti [*Krt2-8* (+/+): *Krt1-19* (−/−)]. (Stained for β-galactosidase with hematoxylin counterstaining.) Note the lesion with the maternal blood (*) and the degenerated allantoic tissue with less vascularization compared with the healthy giant cells and the spongiotrophoblasts in b, d, f and h. In the normal placenta, β-galactosidase (K19) was expressed in the giant cells and the spongiotrophoblasts, but not in the allantois or the labyrinthine trophoblasts. Note the degeneration in the spongiotrophoblasts and the labyrinthine trophoblasts in the compound homozygotes. Arrows in g indicate nucleated embryonic erythrocytes. al, allantois; e, embryonic blood; gc, giant cells; lb, labyrinthine trophoblast; m, maternal blood; sp, spongiotrophoblast. Bars, 100 μm.

lesion was not hemorrhaged as shown by lack of overt clotting (i.e, fibrin network formation), but there was intermixing of the maternal blood with the embryonic blood in the placenta due to the inability of the placenta to keep the circulation systems separate. The embryonic placenta, including the vascular structures, was also deteriorated, and the maternal and embryonic blood cells showed signs of degeneration by 10.5 dpc (data not shown).

On the other hand, staining for another type II cytokeratin K7 in the compound homozygous placenta showed a

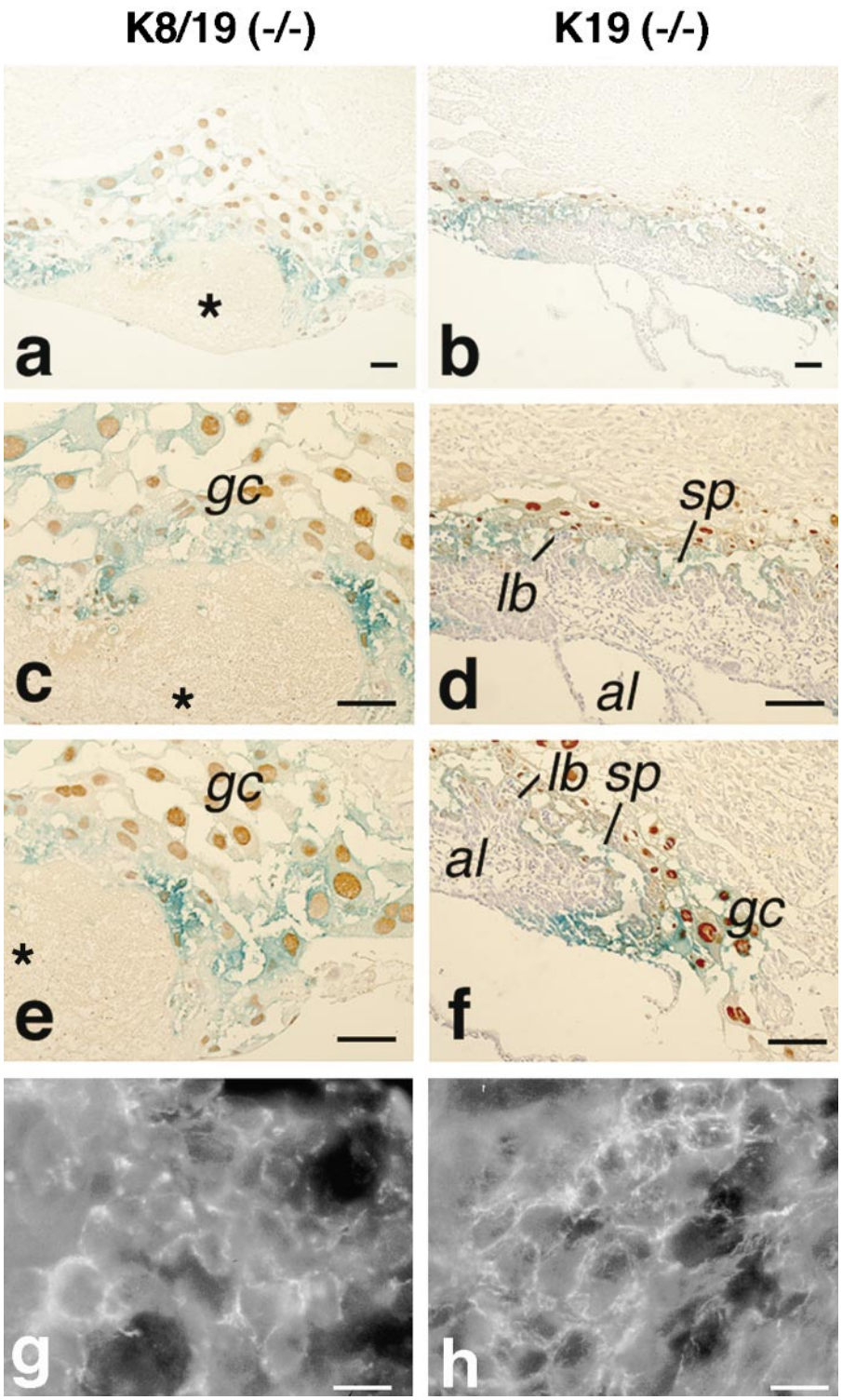

Figure 7. Degeneration of the placenta in the K8/19 compound homozygous concepti at 9.5 dpc; comparison with the K19 homozygous controls. (a–f) Double staining with X-gal for the β-galactosidase activity (greenish blue), and with a specific antibody for Kip2 (brown), followed by a light counterstaining with hematoxylin. Note that the greenish tinge of the blue color for X-gal is due to an electronic enhancement; and that Kip2 is expressed in the nuclei. *The placental lesion; al, allantois; gc, giant cells; lb, labyrinthine trophoblast; and sp, spongiotrophoblast. (g and h) Staining for K7 by indirect immunofluorescence microscopy. Note that image g was electronically enhanced more than h. (Left) Samples of the K8/K19 compound homozygotes [*Krt2-8* (−/−):*Krt1-19* (−/−)]. (Right) Samples of the simple K19 homozygotes [*Krt2-8* (+/+):*Krt1-19* (−/−)]. Bars: (a–f) 100 μm; (g and h) 1 μm.

much weaker immunofluorescence than in the simple K19 homozygotes, and was found essentially in the trophoblasts, but not in the allantoic cells. At a higher magnification, the distribution of K7 in the compound homozygotes was more diffuse than in the K19 homozygotes (Fig. 7, g compared with h). At the same time, a very weak K18 staining was observed in the K8 (−/−)/K19 (−/−) placenta (data not shown). Additional experiments will be needed to confirm the residual K18 and its presumptive partner, which may be K7 or an additional keratin (see Discussion).

Discussion

Our results suggest that the K19 promoter is active in the gut epithelium both in embryos and adults. At ~8.0 dpc, β-galactosidase was expressed in an arch pattern in the posterior embryo. And this expression was soon restricted to the inner wall of the hindgut pocket. If K19 is expressed in the stem cells of the endoderm, this arch-shaped cluster of cells is likely to be the precursor of the hindgut endoderm. Use of the K19 expression as a marker may help un-

derstand the gut differentiation and development in embryos and adults. Taking advantage of this finding, we recently constructed a gene knockin mouse strain in which a bacteriophage P1-derived recombinase gene *cre* was placed under the control of the K19 gene promoter (*Krt1-19^{cre}*). This mouse strain has turned out to be very useful in introducing conditional mutations in a gut-specific manner, because a floxed β-catenin–stabilizing mutation caused thousands of polyps in the intestines of the offspring when crossed with the *Krt1-19^{cre}* mice (Harada et al., 1999).

Type I cytokeratins, K18 and K19 can copolymerize with type II cytokeratins such as K8 and/or K7. Our results suggest that depletion of K19 per se does not interfere with embryonic development or postnatal life in the mouse, even though K19 is expressed at substantial levels in the developing embryo and in the adult. Given the evolutionary conservation of K19 across the vertebrates, it is reasonable to assume that K19 plays an important role that confers a selective advantage. It remains to be investigated whether K19 null mice show changes in such characteristics as tumor development or wound healing. Defects may become apparent in the K19 null mice when they are exposed to a less-protected environment rather than laboratory conditions. The absence of an overt phenotype may be due to compensatory functions of K18, which is coexpressed in the extraembryonic tissues, and K20, which is also coexpressed in the intestine (Moll et al., 1990; Calnek and Quaroni, 1993). If K19 and K8 contribute to the same function, the two mutant alleles should interact genetically. Our results confirmed this prediction: the compound homozygous embryos have a more severe phenotype than embryos deficient in only one of the two genes. In the FVB/N background, >50% of the homozygous K8 null embryos survive to adulthood (Baribault et al., 1993). However, no compound homozygotes were found among >200 newborn pups. This result indicates a marked increase in the penetrance of the lethal phenotype to 100% in the compound homozygotes, possibly at an earlier stage than K8 homozygotes. The compound homozygous embryos have defects in the placenta, the major site of gas and metabolite exchanges between the maternal and fetal blood. The mouse placenta consists of three morphologically distinct trophoblast layers; namely, the labyrinthine trophoblast, spongiotrophoblast, and giant cell layers (Rossant, 1995; Rossant and Croy, 1985). In the compound homozygous placenta, giant trophoblasts were increased in number, whereas the spongiotrophoblasts and labyrinthine trophoblasts were decreased. Failure to properly form the chorioallantoic placenta results in embryonic lethality at midgestation (Cross et al., 1994; Copp, 1995). Recent gene knockout results show that the placental development is controlled by such genes as basic helix-loop-helix transcription factors *Mash2* (Guillemot et al., 1994) and *Hand1* (Riley et al., 1998), orphan nuclear receptor *Errb* (Luo et al., 1997), and *Ets2* (Yamamoto et al., 1998). In FVB/N K8 knockout mice that escape embryonic lethality, partial hepatectomy results in gross structural alterations and explanted hepatocyte death (Loranger et al., 1997). This may reflect hypersensitivity to tumor necrosis factor (TNF), which is moderated by K8 and K18 (Caulin et al., 2000). The primary cause of early embryonic lethality of K8 homozygous mutants is likely due to placental malfunction because, in the B6 background, K8-deficient embryos are rescued by aggregation with tetraploid embryos (Kupriyanov and Baribault, 1998; Baribault, unpublished results). This leads to an intriguing consideration that TNF family cytokines may be involved in the placental abnormalities of both B6 K8-deficient embryos and the FVB/N compound homozygotes described here, because TNF is implicated in trophoblast function (Rasmussen et al., 1999).

Our results indicate that compound K8 and K19 homozygous mutants, in a permissive genetic background for K8 homozygotes, are defective in the development of placental tissues. K8 deficiency results in the complete loss of both K18 and K19 filaments in the liver and yolk sac (Baribault and Oshima, 1991; Baribault et al., 1993). Why is the phenotype of the compound homozygotes more severe than the simple K8 homozygotes? Perhaps K8 is not the only type II keratin functional in the midgestational placenta. Indeed, low levels of K7 are detectable in embryonic placenta in addition to K18 and K19 (Fig. 7). The removal of K8 results in the degradation of K18 and most K19. However, the residual K19 that is polymerized with K7 would remain in the K8 homozygotes, whereas K19 is also removed in the compound homozygotes. The residual weak signal for K7 in the compound homozygotes may be due to K7/K8 heteropolymers.

It is worth noting that K18 null mice are viable, fertile, and show a normal life span. This may be due to compensation by K19. Old K18 null mice, however, develop a distinctive liver pathology with abnormal hepatocytes containing K8 aggregates (Mallory bodies). Additionally, in the K18 null mice, K7 was absent or markedly reduced in the uterus, where K7, 8, 18, and 19 are to be coexpressed. This observation indicates that cytokeratins have distinct assembly characteristics particular to the specific tissues (Magin et al., 1998).

In conclusion, we have constructed a K19 gene knockout mouse strain, the homozygotes of which were viable, fertile, and appeared normal. When the mutation was introduced into a viable K8 gene knockout mouse strain, however, the compound homozygous embryos died in utero due to defects in the placenta. These results indicate that K19 and K8 cooperate in ensuring the normal development of placental tissues.

We thank M. Oshima and Y. Saga for helpful discussions, and R. Kemler for the gift of the TROMA-1, -2, and -3. We also thank N. Sugimoto, R. Nakajima, and H. Oshima for technical assistance.

This work was supported in part by the Joint Research Fund between The University of Tokyo and Banyu Pharmaceutical Co., grants from Monbusho (MESSC) and the Organization for Pharmaceutical Safety and Research of Japan, and grant CA42302 from the National Cancer Institute.

Submitted: 9 June 2000
Revised: 16 August 2000
Accepted: 12 September 2000

References

Bader, B.L., T.M. Magin, M. Hatzfeld, and W.W. Franke. 1986. Amino acid sequence and gene organization of cytokeratin no. 19, an exceptional tail-less intermediate filament protein. *EMBO (Eur. Mol. Biol. Organ.) J.* 5:1865–1875.

Bader, B.L., L. Jahn, and W.W. Franke. 1988. Low level expression of cytokeratin 8, 18 and 19 in vascular smooth muscle cells of human umbilical cord and in cultured cells derived therefrom, with an analysis of the chromosomal locus containing the cytokeratin 19 gene. *Eur. J. Cell Biol.* 47:300–319.

Baribault, H., and R.G. Oshima. 1991. Polarized and functional epithelia can form after the targeted inactivation of both mouse keratin 8 alleles. *J. Cell Biol.* 115:1675–1684.

Baribault, H., J. Price, K. Miyai, and R.G. Oshima. 1993. Mid-gestational le-

thality in mice lacking keratin 8. *Genes Dev*. 7:1191–1202.
Baribault, H., J. Penner, R.V. Iozzo, and M. Wilson-Heiner. 1994. Colorectal hyperplasia and inflammation in keratin 8-deficient FVB/N mice. *Genes Dev*. 8:2964–2973.
Boller, K., R. Kemler, H. Baribault, and T. Doetschman. 1987. Differential distribution of cytokeratins after microinjection of anti-cytokeratin monoclonal antibodies. *Eur. J. Cell Biol*. 43:459–468.
Bosch, F.X., R.E. Leube, T. Achtstätter, R. Moll, and W.W. Franke. 1988. Expression of simple epithelial type cytokeratins in stratified epithelia as detected by immunolocalization and hybridization in situ. *J. Cell Biol*. 106: 1635–1648.
Calnek, D., and A. Quaroni. 1993. Differential localization by in situ hybridization of distinct keratin mRNA species during intestinal epithelial cell development and differentiation. *Differentiation*. 53:95–104.
Caulin, C., C.F. Ware, T.M. Magin, and R.G. Oshima. 2000. Keratin-dependent, epithelial resistance to tumor necrosis factor-independent apoptosis. *J. Cell Biol*. 149:17–22.
Copp, A.J. 1995. Death before birth: clues from gene knockouts and mutations. *Trends Genet*. 11:87–93.
Cross, J.C., Z. Werb, and S.J. Fisher. 1994. Implantation and the placenta: key pieces of the development puzzle. *Science*. 266:1508–1518.
Ecker, R.L. 1988. Sequence of the human 40-kDa keratin reveals an unusual structure with very high sequence identity to the corresponding bovine keratin. *Proc. Natl. Acad. Sci. USA*. 85:1114–1118.
Franke, W.W., C. Grund, C. Kuhn, B.W. Jackson, and K. Illmensee. 1982. Formation of cytoskeletal elements during mouse embryogenesis. III. Primary mesenchymal cells and the first appearance of vimentin filaments. *Differentiation*. 23:43–59.
Fuchs, E. 1994. Intermediate filaments and disease: mutations that cripple cell strength. *J. Cell Biol*. 125:511–516.
Guillemot, F., A. Nagy, A. Auerbach, J. Rossant, and A.L. Joyner. 1994. Essential role of Mash-2 in extraembryonic development. *Nature*. 371:333–336.
Harada, N., Y. Tamai, T. Ishikawa, B. Sauer, K. Takaku, M. Oshima, and M.M. Taketo. 1999. Intestinal polyposis in mice with a dominant stable mutation of the β-catenin gene. *EMBO (Eur. Mol. Biol. Organ.) J*. 18:5931–5942.
Ichinose, Y., K. Hashido, H. Miyamoto, T. Nagata, M. Nozaki, T. Morita, and A. Matsushiro. 1989. Molecular cloning and characterization of cDNA encoding mouse cytokeratin No.19. *Gene (Amst.)*. 80:315–323.
Jackson, B.W., C. Grund, E. Schmidt, K. Burki, W.W. Franke, and K. Illmensee. 1980. Formation of cytoskeletal elements during mouse embryogenesis. Intermediate filaments of the cytokeratin type desmosomes in preimplantation embryos. *Differentiation*. 17:161–179.
Jackson, B.W., C. Grund, S. Winter, W.W. Franke, and K. Illmensee. 1981. Formation of cytoskeletal elements during mouse embryogenesis, II. Epithelial differentiation and intermediate-sized filaments in early postimplantation embryos. *Differentiation*. 20:203–216.
Kasper, M., P. Stosiek, H. Typlt, and U. Karsten. 1987. Histological evaluation of three new monoclonal anti-cytokeratin antibodies. 1. Normal tissues. *Eur. J. Cancer Clin. Oncol*. 23:137–147.
Kaufman, M.H. 1992. The atlas of mouse development. Academic Press, London, UK. 1–15.
Kemler, R., P. Brûlet, M.T. Schnebelen, J. Gaillard, and F. Jacob. 1981. Reactivity of monoclonal antibodies against intermediate filament proteins during embryonic development. *J. Embryol. Exp. Morph*. 64:45–60.
Kulesh, D.A., G. Ceceña, Y.M. Darmon, M. Vasseur, and R.G. Oshima. 1989. Posttranslational regulation of keratins: degradation of mouse and human keratins 18 and 8. *Mol. Cell. Biol*. 9:1553–1565.
Kupriyanov, S., and H. Baribault. 1998. Genetic control of extraembryonic cell lineages studied with tetraploid ↔ diploid chimeric concepti. *Biochem. Cell Biol*. 76:1017–1027.
Lane, E.B., B.L.M. Hogan, M. Kurkinen, and J.I. Garrels. 1983. Co-expression of vimentin and cytokeratins in parietal endoderm cells of early mouse embryo. *Nature*. 303:701–704.
Loranger, A., S. Duclos, A. Grenier, J. Price, M. Wilson-Heiner, H. Baribault, and N. Marceau. 1997. Simple epithelium keratins are required for maintenance of hepatocyte integrity. *Am. J. Pathol*. 151:1673–1683.
Luo, J., R. Sladek, J. Bader, A. Matthyssen, J. Rossant, and V. Giguère. 1997. Placental abnormalities in mouse embryos lacking the orphan nuclear receptor ERR-β. *Nature*. 388:778–782.
Lussier, M., T. Ouellet, C. Lampron, L. Lapointe, and A. Royal. 1989. Mouse keratin 19: complete amino acid sequence and gene expression during development. *Gene*. 85:435–444.
Lussier, M., M. Filion, J.G. Compton, J.H. Nadeau, L. Lapointe, and A. Royal. 1990. The mouse keratin 19-encoding gene: sequence and chromosomal assignment. *Gene*. 95:203–213.
Magin, T.M. 1997. Lessons from keratin transgenic and knockout mice. *In* Subcellular Biochemistry. H. Herrmann and J.R. Harris, editors. Plenum Publishing Corp., London, UK.
Magin, T.M., R. Schröder, S. Leitgeb, F. Wanninger, K. Zatloukal, C. Grund, and D.W. Melton. 1998. Lessons from keratin 18 knockout mice: formation of novel keratin filaments, secondary loss of keratin 7 and accumulation of liver-specific keratin 8-positive aggregates. *J. Cell Biol*. 140:1441–1451.
McLean, W.H., and E.B. Lane. 1995. Intermediate filaments in disease. *Curr. Opin. Cell Biol*. 7:118–125.
Moll, R., W.W. Franke, D.L. Schiller, B. Geiger, and R. Krepler. 1982. The catalog of human cytokeratins: patterns of expression in normal epithelia, tumors and cultured cells. *Cell*. 31:11–24.
Moll, R., D.L. Schiller, and W.W. Franke. 1990. Identification of protein IT of the intestinal cytoskeleton as a novel type I cytokeratin with unusual properties and expression patterns. *J. Cell Biol*. 111:567–580.
Moll, R. 1994. Cytokeratin in the histological diagnosis of malignant tumors. *Int. J. Biol. Markers*. 9:63–69.
Nozaki, M., K. Murata, T. Morita, and A. Matsushiro. 1988. Isolation of ENDO A cDNA from mouse 8-cell stage embryos. *Biochem. Biophys. Res. Commun*. 154:890–894.
Nozaki, M., M. Mori, and A. Matsushiro. 1994. The complete sequence of the gene encoding mouse cytokeratin 15. *Gene*. 138:197–200.
Oshima, N., H. Oshima, K. Kitagawa, M. Kobayashi, C. Itakura, and M. Taketo. 1995. Loss of *Apc* heterozygosity and abnormal tissue building in nascent intestinal polyps in mice carrying a truncated *Apc* gene. *Proc. Natl. Acad. Sci. USA*. 92:4482–4486.
Pujol, J.L., J. Grenier, J.P. Daurès, A. Daver, H. Pujol, and F.B. Michel. 1993. Serum fragment of cytokeratin subunit 19 measured by CYFRA 21-1 immunoradiometric assay as a marker of lung cancer. *Cancer Res*. 53:61–66.
Quinlan, R.A., D.L. Schiller, M. Hatzfeld, T. Achtstätter, R. Moll, J.L. Jorcano, T.M. Magin, and W.W. Franke. 1985. Patterns of expression and organization of cytokeratin intermediate filaments. *Ann. NY Acad. Sci*. 455:282–306.
Rasmussen, C.A., J.L. Pace, S. Banerjee, T.A. Phillips, and J.S. Hunt. 1999. Trophoblastic cell lines generated from tumor necrosis factor receptor-deficient mice reveal specific functions for the two tumor necrosis factor receptors. *Placenta*. 20:213–222.
Riley, P., L. Anson-Cartwright, and J.C. Cross. 1998. The Hand1 bHLH transcription factor is essential for placentation and cardiac morphogenesis. *Nat. Genet*. 18:271–275.
Rossant, J., and B.A. Croy. 1985. Genetic identification of tissue of origin of cellular populations within the mouse placenta. *J. Embryol. Exp. Morphol*. 86:177–198.
Rossant, J. 1995. Development of the extraembryonic lineages. *Semin. Dev*. 6:237–247.
Saga, Y., N. Hata, S. Kobayashi, T. Magnuson, M.F. Seldin, and M.M. Taketo. 1996. MesP1: a novel basic helix-loop-helix protein expressed in the nascent mesodermal cells during mouse gastrulation. *Development*. 122:2769–2778.
Shull, M., I. Ormsby, A.B. Kier, S. Pawlowski, R.J. Diebold, M. Yin, R. Allen, C. Sidman, G. Proetzel, D. Calvin, N. Annunziata, and T. Doetschman. 1992. Targeted disruption of the mouse transforming growth factor-b1 gene results in multifocal inflammatory disease. *Nature*. 359:693–699.
Soriano, P., C. Montgomery, R. Geske, and A. Bradley. 1991. Targeted disruption of the c-*src* proto-oncogene leads to osteoporosis in mice. *Cell*. 64:693–702.
Stasiak, P.C., P.E. Purkis, I.M. Leigh, and E.B. Lane. 1989. Keratin 19: predicted amino acid sequence and broad tissue distribution suggest it evolved from keratinocyte keratins. *J. Invest. Dermatol*. 92:707–716.
Steinert, P.M., and D.R. Roop. 1988. Molecular and cellular biology of intermediate filaments. *Annu. Rev. Biochem*. 57:593–625.
Sun, T.-T., R. Eichner, A. Schermer, D. Cooper, W.G. Nelson, and R.A. Weiss. 1984. Classification, expression, and possible mechanisms of evolution of mammalian keratins: a unifying model. *In* Cancer Cells I, the Transformed Phenotype. A.J. Levine, G.F. Vande Woude, W.C. Topp, and J.D. Watson, editors. Cold Spring Harbor Laboratory Press, Cold Spring Harbor, NY. 169–176.
Takemoto, Y., Y. Fujimura, M. Matsumoto, Y. Tamai, T. Morita, A. Matsushiro, and M. Nozaki. 1991. The promoter of the *endo* A cytokeratin gene is activated by a 3′ downstream enhancer. *Nucleic Acids Res*. 19:2761–2765.
Tamai, Y., Y. Takemoto, M. Matsumoto, T. Morita, A. Matsushiro, and M. Nozaki. 1991. Sequence of the *Endo* A gene encoding mouse cytokeratin and its methylation state in the CpG-rich region. *Gene*. 104:169–176.
Vassar, R., P.A. Coulombe, L. Degenstein, K. Albers, and E. Fuchs. 1991. Mutant keratin expression in transgenic mice causes marked abnormalities resembling a human genetic skin disease. *Cell*. 64:365–380.
Wu, Y.-J., and J.G. Rheinwald. 1981. A new small (40 kd) keratin filament protein made by some cultured human squamous cell carcinomas. *Cell*. 25:627–635.
Yamamoto, H., M.L. Flannery, S. Kupriyanov, J. Pearce, S.R. McKercher, G.W. Henkel, R.A. Maki, Z. Werb, and R.G. Oshima. 1998. Defective trophoblast function in mice with a targeted mutation of Ets2. *Genes Dev*. 12: 1315–1326.